From Colloidal Monodisperse Nickel Nanoparticles to Well-Defined Ni/Al_2O_3 Model Catalysts

Eirini Zacharaki[†], *Pablo Beato*[‡], *Ramchandra R. Tiruvalam*[‡], *Klas J. Andersson*[‡], *Helmer Fjellvåg*[†], *and Anja O. Sjåstad*[*†]

[†] Department of Chemistry, Center for Materials Science and Nanotechnology, University of Oslo, P.O. Box 1033 Blindern, N-0315 Oslo, Norway

[‡] Haldor Topsoe A/S, Haldor Topsøes Allé 1, DK-2800 Kongens Lyngby, Denmark

ABSTRACT

In the past few decades, advances in colloidal nanoparticle synthesis have created new possibilities for the preparation of supported model catalysts. However, effective removal of surfactants is a prerequisite to evaluate the catalytic properties of these catalysts in any reaction of interest. Here we report on the colloidal preparation of surfactant-free Ni/Al_2O_3 model catalysts. Monodisperse Ni nanoparticles (NPs) with mean particle size ranging from 4 to 9 nm were synthesized via thermal decomposition of a zerovalent precursor in the presence of oleic acid. Five weight percent Ni/Al_2O_3 catalysts were produced by direct deposition of the presynthesized NPs on an alumina support, followed by thermal activation (oxidation–

reduction cycle) for complete surfactant removal and surface cleaning. Structural and morphological characteristics of the nanoscale catalysts are described in detail following the propagation of the bulk and surface Ni species at the different treatment stages. Powder X-ray diffraction, electron microscopy, and temperature-programmed reduction experiments as well as infrared spectroscopy of CO adsorption and magnetic measurements were conducted. The applied thermal treatments are proven to be fully adequate for complete surfactant removal while preserving the metal particle size and the size distribution at the level attained by the colloidal synthesis. Compared with standard impregnated Ni/Al_2O_3 catalysts, the current model materials display narrowed Ni particle size distributions and increased reducibility with a higher fraction of the metallic nickel atoms exposed at the catalyst surface.

INTRODUCTION

Industrial chemical and petrochemical processes are constantly being optimized to meet global growing demands for the production of energy, fine chemicals, food, and other high technology products. Most chemical processes depend on the use of one or more solid catalysts, often composed of metal nanoparticles (NPs) supported on inorganic oxide carriers.[1] These catalysts are produced by simple synthetic procedures with limited control over their nanostructuring, and consequently it is difficult to establish synthesis–structure–performance relationships. Therefore, fundamental studies are conducted on well-defined two- or three-dimensional (2D or 3D) model catalysts, wherein essential parameters, such as metal particle size, morphology, chemical composition, atomic arrangement and metal dispersion, are strictly controlled.

Recent advances in metal NP colloidal synthesis offer a promising and attractive way for preparing 3D supported NP-based model catalysts. Monodisperse metal NPs can be obtained by means of colloidal chemistry, wherein their size, shape, and composition can be finely controlled.[2-4] Controlled deposition of these metal colloids on a vast variety of carriers can yield exceptionally high and uniform dispersion of metal with controllable metal loadings. Moreover, the direct formation of metal NPs via colloidal chemistry breaks the so-called dispersion–reducibility dependence[5] which inherently exists in transition-metal catalysts prepared from oxide precursors and suppresses the formation of poorly reducible substances, such as transition-metal silicates, aluminates and titanates.[6]

However, while considering this two-step colloidal synthesis, one notes that further development is required in respect of the synthesis of metal colloids free from synthesis residues. For example, Carenco et al.[7] produced monodisperse Ni NPs with a tunable particle size ranging from 2 to 30 nm using alkylamine- and phosphine-containing surfactants. However, such synthetic protocols may not be suitable for model Ni-based catalysts as P doping takes place when phosphine-containing surfactants are used.[8-9] To inhibit contamination of the colloidal metal NPs by synthesis residues, a more targeted strategy would be the use of surfactants containing C, O and N only. Oleic acid is one of the most frequently applied surfactants for colloidal NP synthesis, also used in impregnation protocols for the preparation of supported NPs.[10-11] In the case of Ni-based colloidal synthesis, several protocols have been reported wherein oleic acid is used either solely or in combination with other (excluding P-containing) surfactants.[12-16] None of these works achieved particle size control in the 1–10 nm range. Therefore, synthetic protocols that yield size-tunable Ni NPs without any chemical contamination that may affect reactivity are highly desirable.

The second important aspect within colloidal preparation of model catalysts is the removal of organic matter from the NPs surfaces prior to catalysis,[17-19] as it may block catalytically active

sites[17, 20] and inhibit catalytic activity.[21] From an application point of view, it is therefore crucial to establish proper procedures of surfactant removal and surface cleaning without influencing the particle size and morphology. During the last decade, a flurry of efforts have been directed toward the preparation of supported colloidal metal NP catalysts, and several methods for surfactant removal have been examined.[19, 21] However, most of these studies are conducted on catalysts containing either platinum group metals[17, 22-23] or gold.[24] On the contrary, the removal of surfactants is rarely studied in earth-abundant metal systems and deserves more attention.

Due to their low cost and abundant metal resources, supported Ni catalysts are considered as promising candidates in a number of processes, in particular hydrogenation and reforming reactions.[25-27] Despite the industrial importance of Ni catalysts, studies on the utilization of the colloidal approach for the preparation of supported Ni NP-based catalyst are limited and have reported that it is rather ineffective. For example, Rinaldi et al.[28] prepared silica-supported colloidal Ni NPs for hydrogenation of cyclohexene and ethanol steam reforming. The catalytic activity was low and attributed to incomplete surfactant removal.[28]

Here, we report on the preparation of surfactant-free Ni/Al_2O_3 catalysts by the colloidal approach. We target Ni NPs in the sub 10 nm size regime using P-free surfactants. The Ni colloids are deposited on Al_2O_3 with a spherical morphology, which is ideal for electron microscopy imaging. A key in these efforts is application of prolonged thermal treatments (oxidation–reduction cycle) at suited temperatures for complete surfactant removal while avoiding particle sintering. The obtained catalysts are characterized in detail with respect to their structural and morphological characteristics, as well as with respect to bulk and surface species prevailing at different stages of the treatments, and discussed in comparison with an impregnated catalyst.

EXPERIMENTAL SECTION

Colloidal Ni NP Synthesis. Ni NPs were obtained under inert conditions by heat-up[29] based thermolysis of bis(1,5-cyclooctadiene)nickel(0), $Ni(cod)_2$, in toluene (C_7H_8, 99.8%, anhydrous) with oleic acid (OA, $C_{18}H_{34}O_2$, ≥99%) as the surfactant, inspired by the method reported by Cheng et al.[13] Typically, a one-pot synthesis batch was prepared in a 250 mL three-neck round-bottom flask by dissolving 0.4 g $Ni(cod)_2$ in 15 mL toluene containing 15–40 μL OA. A colloidal suspension was formed when the reaction mixture was heated at refluxing conditions (T ≈110 °C) under vigorous stirring in an Ar (5 N, Aga) atmosphere. The formed suspension was aged at 110 °C for 30 min before being quenched in 10 mL of toluene. The NPs were flocculated with excess 2-propanol (C_3H_8O, 99.5%, anhydrous) and isolated by centrifugation. After the supernatant was discarded, the NP precipitate was cleaned by three repetitive washing (with 2-propanol)–centrifugation cycles, redispersed in 10 mL of hexane (C_6H_{14}, 95%, anhydrous), and stored inertly. All reagents were supplied by Sigma-Aldrich and used without further purification.

Catalyst Preparation. The 5 wt % Ni/Al_2O_3-x (x denotes mean NP size; 5 or 9 nm) model catalysts were prepared as follows: A 1.2 g mass of non-porous Al_2O_3 (99.5%, NanoDur, Alfa Aesar) with a spherical morphology, mean particle size of ~50 nm, a phase composition of δ (70) and γ (30), and a specific surface area of 37 m^2/g, was conditioned at 650 °C in air for 10 h, added to 10 mL of hexane, and sonicated for 1 h before being mixed with the relevant Ni NP dispersion. The resulting suspension was stirred at 20 °C under inert conditions for 16 h. Thereafter, the solvent was evaporated at 20 °C in an Ar flow, and the obtained product dried at 80 °C. Samples from this preparation stage are denoted 'untreated'. Untreated Ni/Al_2O_3 catalysts were oxidized in air at 450 °C for 5 h and reduced in 5 vol % H_2/ N_2 at 400 °C for 4 h, unless stated otherwise. A reference sample, denoted 'Ni/Al_2O_3-I', was prepared by conventional impregnation with nickel(II) nitrate salt (see the extended experimental details

given in the Supporting Information) and activated (via oxidation–reduction) similarly to the colloidal prepared catalysts, facilitating direct comparison of the preparation methodologies.

Characterization. Transmission electron microscopy (TEM) images were collected on a Philips CM200 microscope operated at 200 kV. Mean particle sizes (diameter of spherical particles or the largest projected cross section for supported NPs) and the associated standard deviation were determined using ImageJ[30] by analysis of at least 200–300 particles. Powder X-ray diffraction (PXRD) patterns were acquired on a Bruker D8 Venture diffractometer using Mo Kα radiation. Unit cell dimensions and mean crystallite sizes were extracted from structureless pattern profile refinements[31] using the TOPAS[32] software package. Dynamic light scattering (DLS) data were collected on a Malvern Zetasizer (Nano series ZS, Malvern Instruments). The content of metallic nickel (degree of reduction) in reduced samples was quantified according to the procedure described by Karthikeyan et al.,[33] using magnetic data collected on a Quantum Design physical property measurement system (PPMS, model 6000) for magnetic fields up to 6 Tesla. The total nickel loading of the catalysts was determined using inductively coupled optical emission spectrometry (ICP-OES, Agilent 720). Fourier transform infrared (FTIR) spectra of adsorbed CO were collected on a Bruker FTIR spectrometer (Vertex 70) equipped with a mercury–cadmium–telluride (MCT) cryodetector. Prior to CO adsorption experiments, samples were in situ reduced at 400 °C for 2h in diluted hydrogen. Raman spectra were obtained using a LabRAM confocal microscope (Horriba/Jobin Yvon) equipped with a He–Ne laser. Temperature-programmed oxidation (TPO) and reduction (H_2-TPR) experiments in synthetic air and 5 vol % H_2 in N_2, were carried out in a Linkam CCR1000 reactor[34] and followed semiquantitatively by mass spectrometry (MS, Omnistar QMG 220 mass spectrometer, Pfeiffer Vacuum). Extended experimental details on PXRD, DLS, FTIR-CO adsorption and Raman spectroscopy are given in the Supporting Information.

RESULTS AND DISCUSSION

Colloidal Ni NP Synthesis. Representative TEM images of the synthesized Ni NPs are given in Figure 1a–c, along with the obtained particle size distributions (Figure 1d). The particles have a quasi-spherical morphology with a relative narrow size distribution (16–22 % variation in diameter). By varying the metal to surfactant (Ni/OA) molar ratio from 5.6 to 31.1, the mean particle size could be reproducibly tuned from 4 to 9 nm. A linear correlation between Ni/OA molar ratio and measured mean particle size is found (Figure 1e), similar to what observed by Zacharaki et al. for Co NPs.[35] Two sets of Ni NPs with discrete, <10% overlapping mean sizes (5 and 9 nm) were produced for catalyst preparation. TEM imaging further indicates that the as-prepared Ni NPs are well dispersed in hexane without significant aggregation, which is also supported by DLS (Figure S1, Supporting Information).

PXRD phase analysis and profile refinements (Figure 2 and Table S1, Supporting Information) show that the as-prepared NPs consist of metallic Ni (cubic close-packed, ccp; a = 0.354 nm) and minor quantities of NiO (NaCl-type structure). The significant peak broadening associated with the NiO Bragg reflections suggests that the oxide resides on the metallic Ni NPs as a result of partial surface oxidation. Assuming a spherical particle shape, the diffraction analyses give crystallite diameters between 2.8 and 7.5 nm for ccp Ni (Table S1). These values are systematically smaller than the measured (by TEM) mean particle sizes, suggesting either that the Ni NPs are passivated by a thin layer of oxide which is not detectable by PXRD or that they are polycrystalline in nature.

We note that our heat-up-based colloidal procedure allows size control in the sub 10 nm size range. The Ni NPs are not hampered by phosphorus doping[8] since we have avoided the use of phosphine-containing surfactants, frequently added to achieve monodisperse Ni nanoparticles[7]. To our knowledge, such a one-pot route without precursor injection, wherein

oleic acid is used as the sole surfactant, has never been reported. The synthesized Ni NPs form stable suspensions in hexane, which provides an excellent starting point for producing highly dispersed Ni/Al_2O_3 catalysts.

Ni/Al_2O_3-I Reference Catalyst. A 7 wt % Ni/Al_2O_3 catalyst was prepared by the conventional impregnation technique with a Ni^0 content of 55%, as quantified from magnetic data (Table 1). PXRD phase analysis (Figure S2, Supporting Information) and profile refinements (not shown) indicate that the reduced Ni/Al_2O_3-I sample consists mainly of metallic Ni (ccp; a = 0.353 nm) with an average crystallite size of ~10 nm. However, scanning transmission electron microscopy (STEM) imaging (Figure S3, Supporting Information) reveals that the sample is highly inhomogeneous, consisting mainly of small 4–10 nm sized particles and bigger agglomerates with sizes in the 20–40 nm range (Figure S4, Supporting Information).

Colloidal Ni/Al_2O_3 Catalysts Preparation and Surfactant Removal. A schematic illustration of the preparation and activation of colloidal Ni/Al_2O_3 model catalysts is shown in Scheme 1. The Ni/Al_2O_3 catalysts were obtained by direct deposition of the presynthesized Ni colloids on alumina. Thereafter, surfactant removal was addressed by thermal activation (via an oxidation–reduction cycle). During oxidation, the Ni NPs transform to NiO with voidlike morphologies due to a Kirkendall-type process (Figure S5, Supporting Information). Similar findings have been reported by Nakamura[36] for unsupported Ni NPs. In the subsequent reduction step, the hollow NiO NPs convert back into dense metallic Ni particles. The nickel loading in the final catalysts, determined by ICP-OES, is close to the nominal content of 5 wt %, Table 1.

An important aspect of catalyst preparation via the colloidal approach is the removal of surfactant(s) from the NP surface prior to catalysis.[17-19] For surfactant removal, thermal

oxidation is by far more effective than plasma and reductive treatments.[17, 19, 21, 28] The treatment temperature is a key factor and precautions must be taken to prevent particle sintering.[18, 37] To identify an effective procedure for surfactant removal, Ni/Al_2O_3-5nm was subjected to TPO–MS, followed by TEM and FTIR experiments to explore size and morphological changes and confirm the removal of surfactant (and its decomposition products). TPO–MS data (not shown) indicate that all organics have decomposed at ca. 280 °C. However, minor residues of organics were evidenced by FTIR even after oxidation at 300 °C for 3 h (see the stretching vibrations of unsaturated C–H bonds at 2957–2858 cm^{-1}, Figures S6a, Supporting Information). On the basis of a trials and error approach, prolonged treatment in air at 450 °C (for 5 h) followed by reduction in H_2 at 400 °C (for 4 h) resulted in completely clean NP surfaces. FTIR and Raman spectroscopies (Figures S6b and S7, Supporting Information) provide proofs of removal of organic molecules.

Representative TEM images show the morphologies of Ni/Al_2O_3-5nm catalyst before (Figure S5a) and after (Figure 3a) the effective thermal treatments. For the untreated catalyst, the Ni NPs arranged uniformly on the alumina while residing apparently loosely bonded on the carrier surface, indicating that the presence of OA ligands restricts their anchoring. After the oxidative–reductive treatments, the Ni NPs become immobilized on the alumina support while maintaining the homogeneous dispersion. Moreover, the Ni NPs preserve their small size and narrow size distribution during the prolonged thermal treatments (see the histogram in Figure 3b). Notably, the particle size distribution is narrower for Ni/Al_2O_3-5nm than for Ni/Al_2O_3-I.

The representative HRTEM image in Figure 4 of reduced Ni/Al_2O_3-5nm shows a 6–8 nm sized supported NP with a core–shell structure. The lattice fringes with d-spacings of 0.204(5) nm and 0.249(8) nm correspond within uncertainty to the (111) planes of ccp Ni[38] and NiO[39],

respectively. Further analyses confirm that metallic nickel NPs are encapsulated by a 2 nm thick NiO shell. This shows that a clean NP Ni surface will easily reoxidize during sample handling. Complementary PXRD data (Figure S8, Supporting Information) show Bragg reflections of both Ni and NiO for these samples. In line with previous reports,[40] no indications for $NiAl_2O_4$ were found in the oxidized nor in the reduced samples.

Successive oxidative–reductive thermal treatments for surfactant removal from NP surfaces have been previously reported,[41-42] but rarely adapted to earth-abundant metals such as Fe, Co and Ni. Such activation procedures, also relevant for catalysts prepared via impregnation,[43] can easily be performed in situ prior to catalysis. These treatments should be performed at adequate temperatures, to not only effectively remove residual species from the catalyst surface, but also suppress particle sintering. As a general rule, temperatures way below the Tammann temperature of the corresponding metal ($T_{Tammann} = 0.5\ T_{melt}$ in kelvin units, ~590 °C for bulk nickel) should be applied. Several strategies including alloying with a higher melting point metal[44] and increasing the metal–support interactions,[45] are capable of mitigating particle growth and inhibiting catalyst deactivation. In the case of Ni/Al_2O_3 catalysts, thermal activation for surfactant removal may lead to the formation of stable $NiAl_2O_4$-type oxides. These mixed oxides, although considered beneficial to enhancing the sintering resistance of the catalyst due to anchoring of the metal NPs on the support,[40] often restrict the catalyst chemical composition and therefore function. Furthermore, we note that under such thermal treatments the Ni NPs undergo severe structural reconstruction (via a Kirkendall-type process) which might affect the as-achieved by the colloidal synthesis structural control (that is, morphology and mixing pattern) of homo- and bimetallic NP systems with a complex architecture.[9]

Reducibility and Surface Species of Ni/Al_2O_3 Catalysts. A critical property to address during catalyst activation is the number of active sites available for catalysis. For the Ni/Al_2O_3

catalysts, this relates to the quantity of metallic nickel atoms at the surface relative to nickel species found in the bulk.[33] We currently determined the metallic Ni content in the reduced catalysts from magnetization data (Table 1). H_2-TPR experiments were carried out to investigate the bulk reducibility of nickel species and metal–support interactions, while FTIR spectroscopy of CO adsorption was applied to determine the surface nickel species in the mildly reduced catalysts.

According to Table 1, the degree of nickel reduction decreases in the order: Ni/Al_2O_3-5nm > Ni/Al_2O_3-9nm > Ni/Al_2O_3-I. Figure 5 presents H_2-TPR profiles along with a Gaussian-type peak deconvolution for three events at ~300 °C, 300–500 °C and ~530 °C. The latter two are ascribed to α- and β-type NiO.[46] The peak at 300 °C is attributed, according to analyses of the CO_2 and H_2O MS signals (Figure S9, Supporting Information), to the reduction of residual carbon species for Ni/Al_2O_3-5nm (Figure 5a) and unsupported NiO for Ni/Al_2O_3-I (Figure 5c). The α-type is ascribed to nanocrystalline NiO with a relatively weak support interaction, while the β-type is interpreted as NiO interacting strongly with the alumina support.[46] None of the samples showed any high-temperature reduction signals (T ≥ 800 °C) that result from either complete encapsulation of NiO by a surface $NiAl_2O_4$-type spinel[46] or from bulk $NiAl_2O_4$ formation. PXRD data also do not indicate formation of a bulk spinel phase (Figure S8, Supporting Information). Quantitative H_2-TPR results are reported in Table 1. The TPR experiments clearly show that the relative abundance of α-type NiO is significantly improved by the colloidal approach. The difficulty in reducing the β-type NiO species has been previously proposed to arise from a low-temperature migration of Al species and partial surface $NiAl_2O_4$-type spinel formation during oxidation at 450 °C.[46] However, as all samples have been oxidized under identical conditions, the difference in the extent of β-type NiO species in Ni/Al_2O_3–I may be attributed to the mode of preparation as a result of Al^{3+}

dissolution during the impregnation process and its subsequent incorporation into NiO particles.[47-49]

FTIR spectra recorded for in situ reduced Ni/Al_2O_3-5nm and Ni/Al_2O_3-9nm after adsorption of CO at equilibrium pressures of 20 mbar at liquid nitrogen temperature are shown in Figure 6. Spectra for alumina and in situ reduced Ni/Al_2O_3-I are included. The evolution of the FTIR spectra under dynamic vacuum is shown in Figure S10, Supporting Information. At high CO coverage (20 mbar) two major adsorption bands at ca. 2179 and 2156 $cm^{-}1$ are observed for all catalysts. The 2179 $cm^{-}1$ band (Figure 6), which is absent for the naked support, is ascribed to Ni^{2+}–carbonyls, and is therefore indicative of incomplete nickel reduction.[50] The bands at 2156 $cm^{-}1$ are assigned to CO interacting with surface hydroxyl groups of the alumina support. For Ni/Al_2O_3-9nm, the bands at 2100–1800 $cm^{-}1$ (inset in Figure S10b) evidence formation of carbonyls of metallic Ni[51] (see the Supporting Information for detailed analysis). These bands are resolved only at low CO coverages for the Ni/Al_2O_3-5nm sample (inset in Figure S10a), and are absent in the spectra of the impregnated catalyst (inset in Figure S10c). The above results reveal that at the selected reduction conditions some Ni ions resistant to reduction remain on the particle surface, being related to the β-type NiO peak in H_2-TPR. The amount of surface Ni^0 in the activated samples varies as Ni/Al_2O_3-9nm >> Ni/Al_2O_3-5nm. By contrast, surface Ni^0 was not detected by FTIR-CO for the impregnated sample.

Our comparison of Ni/Al_2O_3 catalysts prepared by the colloidal and classic impregnation methodologies reveals superiority of the former as concerns the preparation of supported NP-based materials for model catalytic studies. After activation (via an oxidation–reduction cycle), the colloidal Ni/Al_2O_3 catalysts display a uniform metal dispersion while the metal particle size and size distribution are maintained at the levels attained in the preceding colloidal synthesis. In contrast, impregnation yields a highly inhomogeneous sample with

respect to both Ni particle size and metal dispersion. It is generally acknowledged that due to strong metal–support interactions impregnated Ni/Al_2O_3 catalysts of low metal loading show low susceptibility for nickel ions to be reduced to the metallic state.[52-53] In this context, the two-step colloidal method offers an alternative synthetic strategy which yields low metal loading Ni/Al_2O_3 catalysts with a reducibility that so far has been limited to catalysts with larger particles and higher metal content. Furthermore, the colloidal Ni/Al_2O_3 catalysts were found not only to exhibit an increased reducibility behavior owing to the presence of mainly α-type NiO that possesses weak metal–support interactions, but also, as depicted by FTIR-CO spectroscopy, under mild reduction conditions, to display a significantly larger amount of zerovalent Ni on the particle surface, wherein the amount of surface Ni^0 is proportional to particle size.

SUMMARY AND CONCLUSIONS

In the current work, Ni NPs with a narrow size distribution have been synthesized via a heat-up colloidal methodology with oleic acid as the sole surfactant. The method provides size control in the range from 4 to 9 nm by variations in the Ni/OA molar ratio. On the basis of this approach, Ni/Al_2O_3 catalysts with low metal loading (5 wt %) and a narrow size distribution were prepared, with the goal to explore how this methodology could be used for rational design of model catalysts. Complete surfactant removal and activation was achieved by an optimized oxidation–reduction sequence. Thermal oxidation at relative high temperatures followed by reductive activation provided C-free catalyst surfaces while preserving the metal particle size and size distribution at the levels attained in the preceding colloidal synthesis. This methodology is therefore of great importance for fundamental investigations on the effects of particle size and metal–support interactions in heterogeneous catalysis. During the oxidative–reductive thermal treatment, the Ni NPs and their daughter oxide nanoparticles undergo vivid structural reconstructions (via Kirkendall-type processes)

with minor implication on their size and morphology. However, this major reconstruction may have implications in the design of bi- and multimetallic catalytic systems as the individual elements may display different redox and diffusivity properties. Surfactant removal by means of oxidative and reductive thermal treatments is a fruitful topic for further research.

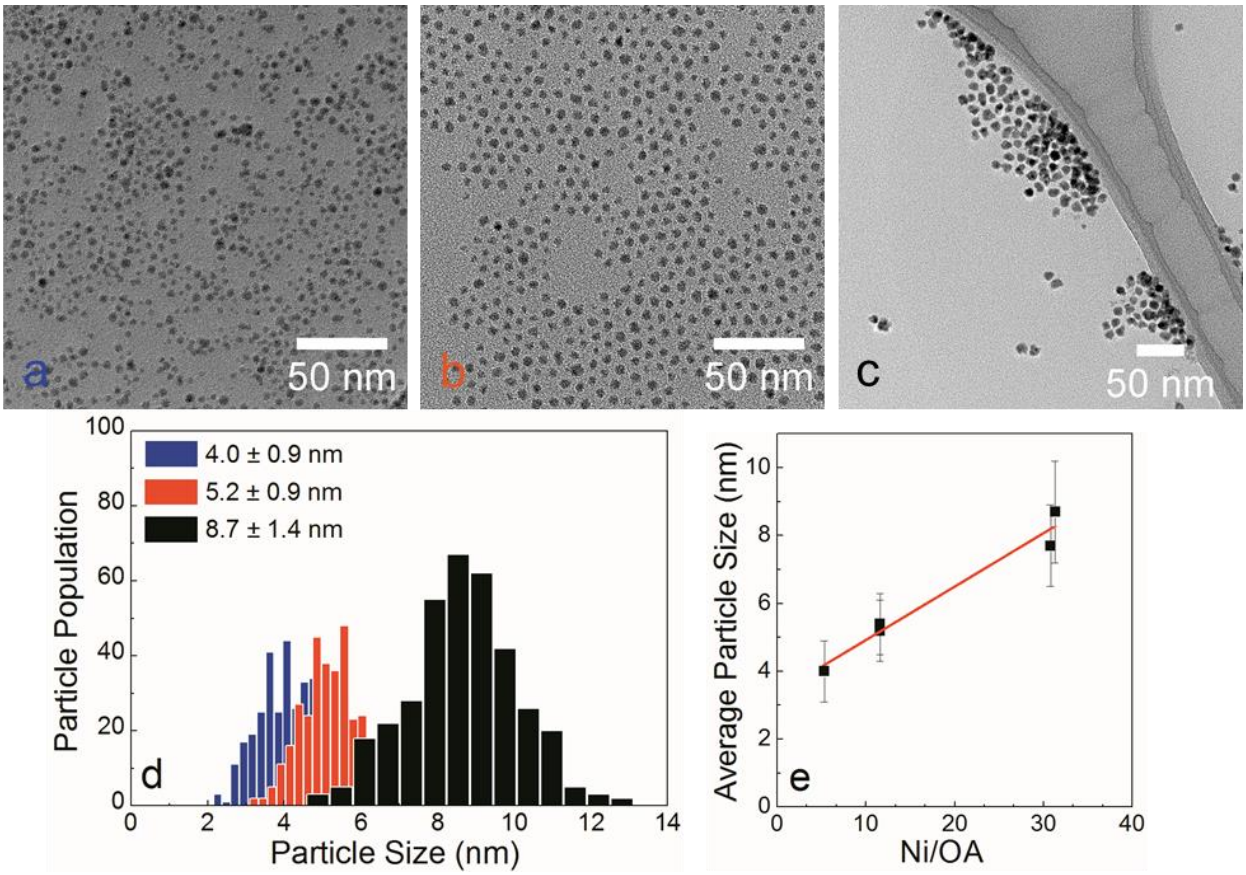

Figure 1. TEM images of Ni NPs of three particle sizes: (a) 4.0; (b) 5.2; and (c) 8.7 nm. (d) Corresponding particle size distributions obtained from counting 300–350 particles. (e) Resultant particle size versus Ni/OA molar ratios.

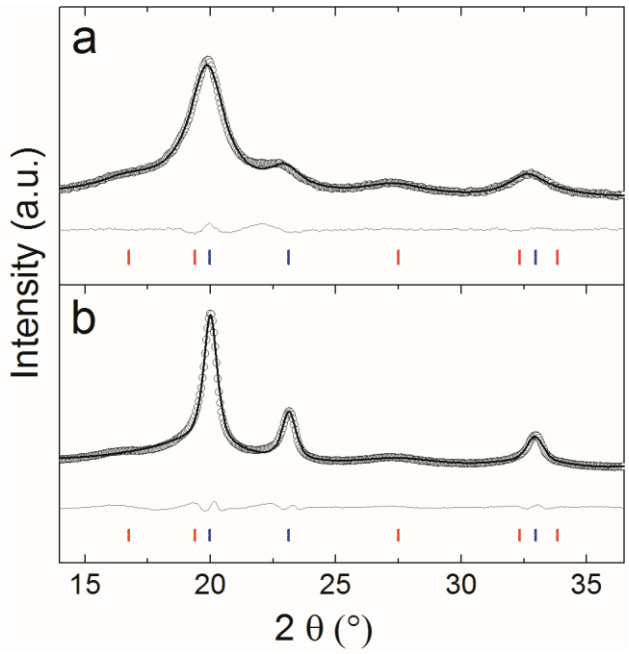

Figure 2. PXRD intensity profiles for NPs synthesized at Ni/OA molar ratios of (a) 11.6; and (b) 31.1. Observed (open symbols), calculated (black line), and difference (gray line) profiles. Positions for Bragg reflections shown with blue and red bars for Ni and NiO, respectively.

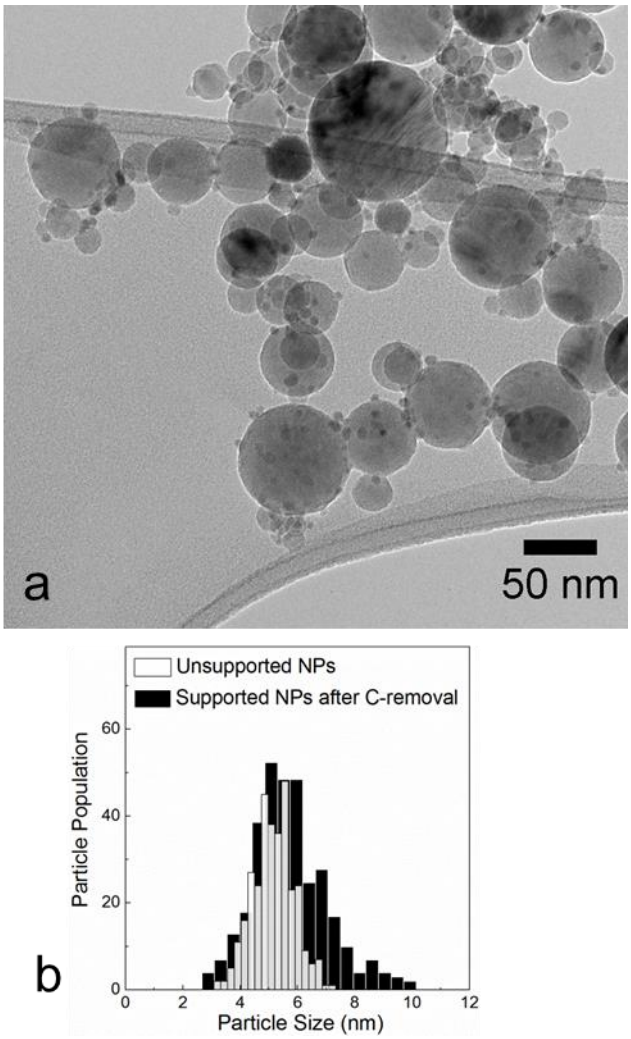

Figure 3. (a) Representative TEM image of reduced Ni/Al_2O_3-5nm (precalcined at 450 °C for 5h) and (b) particle size distributions of unsupported (5.2 ± 0.9 nm, white bars) and supported (5.7 ± 1.3 nm, black bars) NPs of reduced Ni/Al_2O_3-5nm from counting 350 particles.

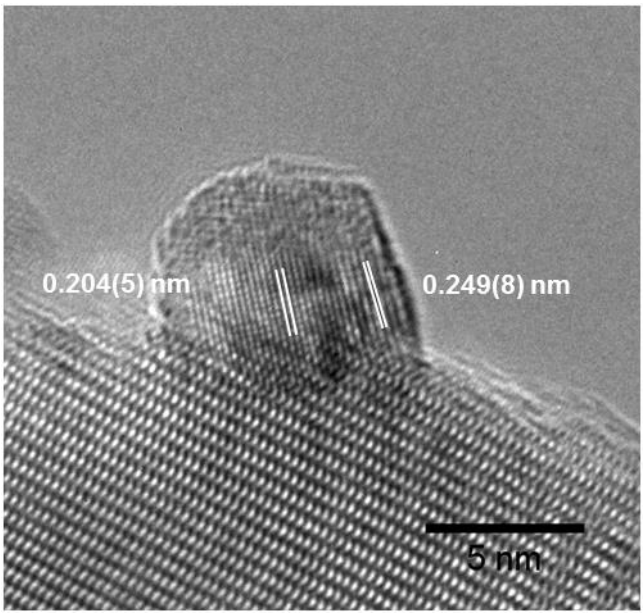

Figure 4. HRTEM image of a supported Ni NP with a NiO passivation layer in the reduced Ni/Al_2O_3-5nm catalyst. Scale bar 5 nm.

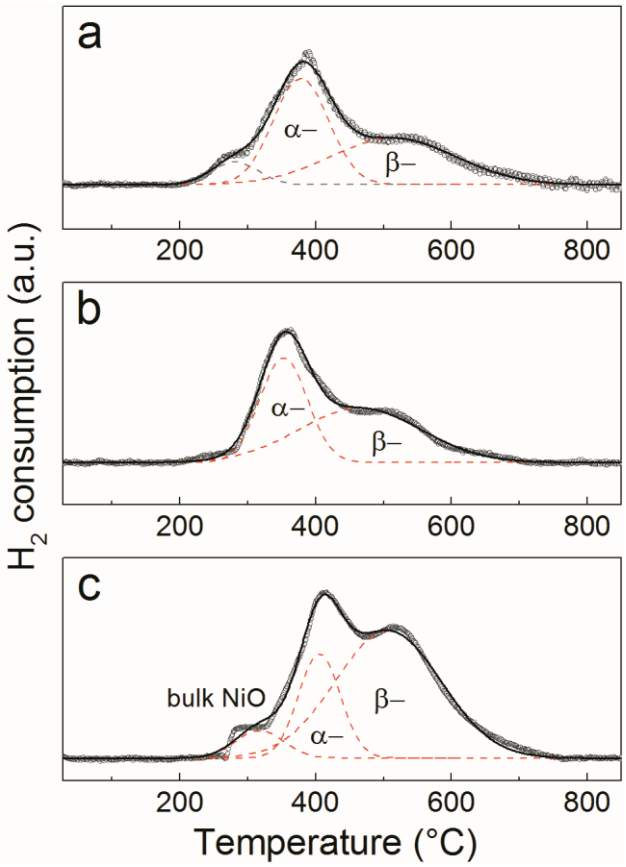

Figure 5. H_2-TPR profiles normalized to the sample weight and fitted with Gaussian deconvolution peaks for all oxidized catalysts: (a) Ni/Al_2O_3-5nm; (b) Ni/Al_2O_3-9nm; (c) Ni/Al_2O_3-I. Samples oxidized at 450 °C for 5h.

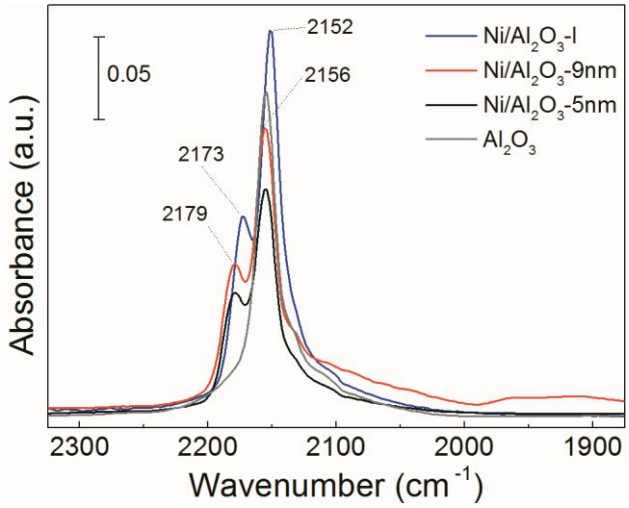

Figure 6. FTIR spectra of CO adsorbed at an equilibrium pressure of 20 mbar and liquid nitrogen temperature for Ni/Al_2O_3 catalysts reduced in situ at 400 °C for 2h.

Scheme 1. Schematic Illustration of the Preparation Procedure of Surfactant-Free Ni/Al_2O_3 Model Catalysts.

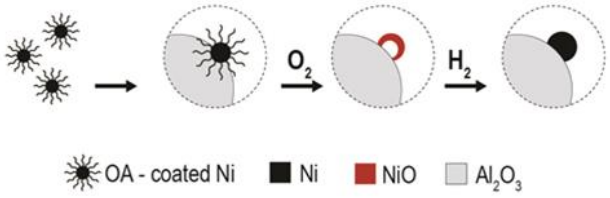

Table 1. Bulk Nickel Species: Total Ni Loading, Ni^0 Content of Reduced Ni/Al_2O_3 Catalysts, and H_2-TPR Quantitative Data.

Catalyst	Total Ni Loading[a] (wt %)	Ni^0 Content[b] (%)	T_{max}[c] of NiO Species (°C)		Relative Abundance of NiO Species[d] (%)		
			α-type	β-type	Bulk	α-type	β-type
Ni/Al_2O_3-I	6.8	55	410	530	7	23	70
Ni/Al_2O_3-5nm	5.3	75	390	550	—	50	50
Ni/Al_2O_3-9nm	3.6	60	360	510	—	43	57

[a]Determined by ICP-OES. Samples reduced at 400 °C for 4h. [b]Degree of reduction quantified from magnetic data. Samples reduced at 400 °C for 4h. [c]Reduction temperatures (T_{max}) from H_2-TPR. Samples oxidized at 450 °C for 5h. [d]Estimated by Gaussian deconvolution of H_2-TPR profiles. he dash indicates "not applicable".

ASSOCIATED CONTENT

Supporting Information.

The Supporting Information is available free of charge on the ACS Publications website at DOI: 10.1021/acs.langmuir.7b02197.

Experimental details, DLS and PXRD of colloidal Ni NPs, TEM images and PXRD of supported Ni catalysts, FTIR and Raman spectra of surfactant-free catalysts, TPR–MS, FTIR-CO, and magnetic data of reduced catalysts (PDF)

AUTHOR INFORMATION

Corresponding Author

* E-mail: a.o.sjastad@kjemi.uio.no

ORCID

Eirini Zacharaki: 0000-0002-3802-2016

Notes

The authors declare no competing financial interest.

ACKNOWLEDGMENT

The technical staff at the Research and Development Division at Haldor Topsoe A/S, Denmark, is gratefully acknowledged. We thank Dr. David Wragg for assistance with X-ray diffraction and Dr. Susmit Kumar for performing the magnetic measurements. This work is part of activities at the inGAP Center of Research-based Innovation, funded by the Research Council of Norway under Contract No. 174893.

REFERENCES

1. Bell, A. T., The Impact of Nanoscience on Heterogeneous Catalysis. *Science* **2003,** *299*, 1688–1691.

2. Na, K.; Zhang, Q.; Somorjai, G. A., Colloidal Metal Nanocatalysts: Synthesis, Characterization, and Catalytic Applications. *J. Cluster Sci.* **2014,** *25*, 83–114.

3. Wu, L.; Mendoza-Garcia, A.; Li, Q.; Sun, S., Organic Phase Syntheses of Magnetic Nanoparticles and Their Applications. *Chem. Rev.* **2016,** *116*, 10473–10512.

4. Gilroy, K. D.; Ruditskiy, A.; Peng, H.-C.; Qin, D.; Xia, Y., Bimetallic Nanocrystals: Syntheses, Properties, and Applications. *Chem. Rev.* **2016,** *116*, 10414–10472.

5. Martínez, A.; Prieto, G., Breaking the Dispersion-Reducibility Dependence in Oxide-Supported Cobalt Nanoparticles. *J. Catal.* **2007,** *245*, 470–476.

6. Yao, N.; Ma, H.; Shao, Y.; Yuan, C.; Lv, D.; Li, X., Effect of Cation-Oligomer Interactions on the Size and Reducibility of NiO Particles on $NiRu/SiO_2$ catalysts. *J. Mater. Chem.* **2011,** *21*, 17403–17412.

7. Carenco, S.; Boissière, C.; Nicole, L.; Sanchez, C.; Le Floch, P.; Mézailles, N., Controlled Design of Size-Tunable Monodisperse Nickel Nanoparticles. *Chem. Mater.* **2010,** *22*, 1340–1349.

8. Moreau, L. M.; Ha, D.-H.; Bealing, C. R.; Zhang, H.; Hennig, R. G.; Robinson, R. D., Unintended Phosphorus Doping of Nickel Nanoparticles during Synthesis with TOP: A Discovery through Structural Analysis. *Nano Lett.* **2012,** *12*, 4530–4539.

9. Carenco, S.; Wu, C.-H.; Shavorskiy, A.; Alayoglu, S.; Somorjai, G. A.; Bluhm, H.; Salmeron, M., Synthesis and Structural Evolution of Nickel–Cobalt Nanoparticles Under H_2 and CO_2. *Small* **2015,** *11*, 3045–3053.

10. Gao, X.; Liu, H.; Hidajat, K.; Kawi, S., Anti-Coking Ni/SiO_2 Catalyst for Dry Reforming of Methane: Role of Oleylamine/Oleic Acid Organic Pair. *ChemCatChem* **2015,** *7*, 4188–4196.

11. Oemar, U.; Kathiraser, Y.; Mo, L.; Ho, X. K.; Kawi, S., CO_2 Reforming of Methane over Highly Active La-promoted Ni Supported on SBA-15 Catalysts: Mechanism and Kinetic Modelling. *Catal. Sci. Technol.* **2016,** *6*, 1173–1186.

12. Bala, T.; Bhame, S. D.; Joy, P. A.; Prasad, B. L. V.; Sastry, M., A Facile Liquid Foam-based Synthesis of Nickel Nanoparticles and their Subsequent Conversion to $Ni_{core}Ag_{shell}$ Particles: Structural Characterization and Investigation of Magnetic Properties. *J. Mater. Chem.* **2004,** *14*, 2941–2945.

13. Cheng, G.; Puntes, V. F.; Guo, T., Synthesis and Self-assembled Ring Structures of Ni Nanocrystals. *J. Colloid Interface Sci.* **2006,** *293*, 430-436.

14. Tzitzios, V.; Basina, G.; Gjoka, M.; Alexandrakis, V.; Georgakilas, V.; Niarchos, D.; Boukos, N.; Petridis, D., Chemical Synthesis and Characterization of Hcp Ni Nanoparticles. *Nanotechnology* **2006,** *17*, 3750–3755.

15. Jayakumar, O. D.; Salunke, H. G.; Tyagi, A. K., Synthesis and Characterization of Stoichiometric NiCo Nanoparticles Dispersible in both Aqueous and Non-aqueous Media. *Solid State Commun.* **2009,** *149*, 1769–1771.

16. He, X.; Zhong, W.; Au, C.-T.; Du, Y., Size Dependence of the Magnetic Properties of Ni Nanoparticles Prepared by Thermal Decomposition Method. *Nanoscale Res. Lett.* **2013,** *8*, 446.

17. Li, D.; Wang, C.; Tripkovic, D.; Sun, S.; Markovic, N. M.; Stamenkovic, V. R., Surfactant Removal for Colloidal Nanoparticles from Solution Synthesis: The Effect on Catalytic Performance. *ACS Catal.* **2012,** *2*, 1358–1362.

18. Zaera, F., New Challenges in Heterogeneous Catalysis for the 21st Century. *Catal. Lett.* **2012,** *142*, 501–516.

19. Niu, Z.; Li, Y., Removal and Utilization of Capping Agents in Nanocatalysis. *Chem. Mater.* **2014,** *26*, 72–83.

20. Crespo-Quesada, M.; Andanson, J.-M.; Yarulin, A.; Lim, B.; Xia, Y.; Kiwi-Minsker, L., UV–Ozone Cleaning of Supported Poly(vinylpyrrolidone)-Stabilized Palladium Nanocubes: Effect of Stabilizer Removal on Morphology and Catalytic Behavior. *Langmuir* **2011,** *27*, 7909–7916.

21. Sonstrom, P.; Baumer, M., Supported Colloidal Nanoparticles in Heterogeneous Gas Phase Catalysis: On the Way to Tailored Catalysts. *Phys. Chem. Chem. Phys.* **2011,** *13*, 19270–19284.

22. Zhao, Y.; Jia, L.; Medrano, J. A.; Ross, J. R. H.; Lefferts, L., Supported Pd Catalysts Prepared via Colloidal Method: The Effect of Acids. *ACS Catal.* **2013,** *3*, 2341–2352.

23. Naresh, N.; Wasim, F. G. S.; Ladewig, B. P.; Neergat, M., Removal of Surfactant and Capping Agent from Pd Nanocubes (Pd-NCs) using Tert-butylamine: Its Effect on Electrochemical Characteristics. *J. Mater. Chem. A* **2013,** *1*, 8553–8559.

24. Comotti, M.; Li, W.-C.; Spliethoff, B.; Schüth, F., Support Effect in High Activity Gold Catalysts for CO Oxidation. *J. Am. Chem. Soc.* **2006,** *128*, 917–924.

25. Adkins, H.; Cramer, H. I., The Use of Nickel as a Catalyst for Hydrogenation. *J. Am. Chem. Soc.* **1930,** *52*, 4349–4358.

26. Rostrup-Nielsen, J. R.; Sehested, J.; Nørskov, J. K., Hydrogen and Synthesis Gas by Steam- and CO_2 Reforming. *Adv. Catal.* **2002,** *47*, 65–139.

27. Gao, J.; Liu, Q.; Gu, F.; Liu, B.; Zhong, Z.; Su, F., Recent Advances in Methanation Catalysts for the Production of Synthetic Natural Gas. *RSC Adv.* **2015,** *5*, 22759–22776.

28. Rinaldi, R.; Porcari, A. d. M.; Rocha, T. C. R.; Cassinelli, W. H.; Ribeiro, R. U.; Bueno, J. M. C.; Zanchet, D., Construction of Heterogeneous Ni Catalysts from Supports and Colloidal Nanoparticles – A Challenging Puzzle. *J. Mol. Catal. A: Chem.* **2009,** *301*, 11–17.

29. van Embden, J.; Chesman, A. S. R.; Jasieniak, J. J., The Heat-Up Synthesis of Colloidal Nanocrystals. *Chem. Mater.* **2015,** *27*, 2246–2285.

30. Schneider, C. A.; Rasband, W. S.; Eliceiri, K. W., NIH Image to ImageJ: 25 years of Image Analysis. *Nat. Methods* **2012,** *9*, 671–675.

31. Pawley, G., Unit-cell Refinement from Powder Diffraction Scans. *J. Appl. Crystallogr.* **1981,** *14*, 357–361.

32. Coelho, A. A., *TOPAS-Academic, Version 4.1 (computer software)*. Publisher: Coelho Software, Brisbane, 2007.

33. Karthikeyan, J.; Song, H.; Olsbye, U.; Fjellvåg, H.; Sjåstad, A. O., Supported Nickel Based Catalysts, Ni/Mg(Al)O, for Natural Gas Conversion, Prepared via Delamination and Restacking of MgAl- and NiAl-Nanosheets. *Top. Catal.* **2015,** *58*, 877–886.

34. Beato, P.; Schachtl, E.; Barbera, K.; Bonino, F.; Bordiga, S., Operando Raman Spectroscopy Applying Novel Fluidized Bed Micro-reactor Technology. *Catal. Today* **2013,** *205*, 128–133.

35. Zacharaki, E.; Kalyva, M.; Fjellvåg, H.; Sjåstad, A. O., Burst Nucleation by Hot Injection for Size Controlled Synthesis of ε-Cobalt Nanoparticles. *Chem. Cent. J* **2016,** *10*, 10.

36. Nakamura, R.; Lee, J. G.; Mori, H.; Nakajima, H., Oxidation Behaviour of Ni Nanoparticles and Formation Process of Hollow NiO. *Philos. Mag.* **2008,** *88*, 257–264.

37. Huang, W.; Hua, Q.; Cao, T., Influence and Removal of Capping Ligands on Catalytic Colloidal Nanoparticles. *Catal. Lett.* **2014,** *144*, 1355–1369.

38. van Ingen, R. P.; Fastenau, R. H. J.; Mittemeijer, E. J., Laser Ablation Deposition of Cu-Ni and Ag-Ni Films: Nonconservation of Alloy Composition and Film Microstructure. *J. Appl. Phys.* **1994,** *76*, 1871–1883.

39. Ghosh, M.; Biswas, K.; Sundaresan, A.; Rao, C. N. R., MnO and NiO Nanoparticles: Synthesis and Magnetic Properties. *J. Mater. Chem.* **2006,** *16*, 106–111.

40. Zhou, L.; Li, L.; Wei, N.; Li, J.; Basset, J.-M., Effect of $NiAl_2O_4$ Formation on Ni/Al_2O_3 Stability during Dry Reforming of Methane. *ChemCatChem* **2015,** *7*, 2508–2516.

41. Lang, H.; May, R. A.; Iversen, B. L.; Chandler, B. D., Dendrimer-Encapsulated Nanoparticle Precursors to Supported Platinum Catalysts. *J. Am. Chem. Soc.* **2003,** *125*, 14832–14836.

42. Xie, T.; Shi, L.; Zhang, J.; Zhang, D., Immobilizing Ni Nanoparticles to Mesoporous Silica with Size and Location Control via a Polyol-assisted Route for Coking- and Sintering-resistant Dry Reforming of Methane. *Chem. Commun.* **2014,** *50*, 7250–7253.

43. Munnik, P.; de Jongh, P. E.; de Jong, K. P., Recent Developments in the Synthesis of Supported Catalysts. *Chem. Rev.* **2015,** *115*, 6687–6718.

44. Morales-Cano, F.; Lundegaard, L. F.; Tiruvalam, R. R.; Falsig, H.; Skjøth-Rasmussen, M. S., Improving the Sintering Resistance of Ni/Al_2O_3 Steam-Reforming Catalysts by Promotion with Noble Metals. *Appl. Catal., A* **2015,** *498*, 117–125.

45. Montes, M.; Soupart, J.-B.; de Saedeleer, M.; Hodnett, B. K.; Delmon, B., Influence of Metal-Support Interactions on the Stability of Ni/SiO_2 Catalysts during Cyclic Oxidation-Reduction Treatments. *J. Chem. Soc., Faraday Trans. 1* **1984,** *80*, 3209–3220.

46. Lundegaard, L. F.; Tiruvalam, R. R.; Tyrsted, C.; Carlsson, A.; Morales-Cano, F.; Ovesen, C. V., Migrating Al Species Hindering NiO Reduction on Al Containing Catalyst Carriers. *Catal. Today* **2016,** *272*, 25–31.

47. Richardson, J. T.; Lei, M.; Turk, B.; Forster, K.; Twigg, M. V., Reduction of Model Steam Reforming Catalysts: $NiO/\alpha\text{-}Al_2O_3$. *Appl. Catal., A* **1994,** *110*, 217–237.

48. Molina, R.; Poncelet, G., α-Alumina-Supported Nickel Catalysts Prepared with Nickel Acetylacetonate. 2. A Study of the Thermolysis of the Metal Precursor. *J. Phys. Chem. B* **1999,** *103*, 11290–11296.

49. Bentaleb, F.; Marceau, E., Influence of the Textural Properties of Porous Aluminas on the Reducibility of Ni/Al_2O_3 Catalysts. *Microporous Mesoporous Mater.* **2012,** *156*, 40–44.

50. Moussa, S.; Arribas, M. A.; Concepción, P.; Martínez, A., Heterogeneous Oligomerization of Ethylene to Liquids on Bifunctional Ni-based Catalysts: The Influence of Support Properties on Nickel Speciation and Catalytic Performance. *Catal. Today* **2016,** *277*, 78–88.

51. Hadjiivanov, K.; Mihaylov, M.; Klissurski, D.; Stefanov, P.; Abadjieva, N.; Vassileva, E.; Mintchev, L., Characterization of Ni/SiO_2 Catalysts Prepared by Successive Deposition and Reduction of Ni^{2+} Ions. *J. Catal.* **1999,** *185*, 314–323.

52. Rynkowski, J. M.; Paryjczak, T.; Lenik, M., On the Nature of Oxidic nickel Phases in $NiO/\gamma\text{-}Al_2O_3$ Catalysts. *Appl. Catal., A* **1993,** *106*, 73–82.

53. Li, C.; Chen, Y.-W., Temperature-programmed-reduction Studies of Nickel Oxide/Alumina Catalysts: Effects of the Preparation Method. *Thermochim. Acta* **1995,** *256*, 457–465.